Nanoscale

Cite this: *Nanoscale*, 2012, **4**, 6307

www.rsc.org/nanoscale

PAPER

Size-dependent melting behavior of iron nanoparticles by replica exchange molecular dynamics

Qiang Shu,[a] Yang Yang,[a] Ying-teng Zhai,[a] D. Y. Sun,[b] H. J. Xiang[a] and X. G. Gong[a]

Received 9th April 2012, Accepted 24th July 2012
DOI: 10.1039/c2nr30853c

Using the replica-exchange molecular dynamics method (REMD), we have investigated the size dependence of the melting behavior of iron nanoparticles. Comparing to conventional molecular dynamics (MD), the REMD method is found to be very efficient in determining the melting point by avoiding superheating and undercooling phenomena. With accurate determination of the melting point, we find that the melting temperature does not follow linearly with the inverse of size. By incorporating the size dependent thickness of surface liquid layer which is observed in our simulation, we propose a revised liquid skin melting model to describe the size dependent melting temperature.

I. Introduction

Due to the finite size effect, nanoparticles exhibit unique physical, chemical, and magnetic properties.[1,2] Compared to bulk materials, the large surface/volume ratio of nanoparticles could lead to more complicated atomic and electronic behavior, thus the thermodynamic properties can also very interesting. In the last a few decades, as one of the fundamental problems in the nanoscience, the melting behavior of nanoparticles has been widely investigated by numerous experimental[3–9] and theoretical[10–17] studies.

Theoretically, the first thermodynamic melting model was established by Pawlow,[18] who also attempted to confirm his own model in the experiment.[19] Subsequently, various thermodynamic models[20–25] were proposed to describe the relationship between the melting point and the size of nanoparticles. Among them, the homogeneous melting (HGM) model[18,20,26] and liquid skin melting (LSM)[21,26] model are widely discussed. The HGM model assumes that the melting occurs homogeneously through the whole of the nanoparticles. Based on the thermodynamics equilibrium between solid state and liquid state at melting point, the relationship of the melting point and the size of nanoparticles can be expressed as $T_{cm}/T_{bm} = 1 - \beta_{HGM}/R$, where T_{cm} is the melting point of nanoparticles, T_{bm} is the melting point of the corresponding bulk material, R is the radius of the nanoparticles, β_{HGM} is a material constant. In contrast to the HGM model, the LSM model, by incorporating the surface melting, assumes the nanoparticles (with total radius R) are composed of an inner core of radius $R - \sigma$ and an outer liquid shell of thickness σ which is usually used as a constant. The expression for the melting point T_{cm} of nanoparticles in the LSM model is given by $T_{cm}/T_{bm} = 1 - \beta_{LSM}/(R - \sigma)$, where β_{LSM} is also a material constant. β_{HGM} and β_{LSM} are different for various materials. We can see that T_{cm} depends linearly on $1/R$ in the HGM model but non-linearly in the LSM model, which is due to the existence of surface melting in the LSM model. In the LSM model, the surface melting appears when the temperature is below the melting point and a sudden melting takes place when the temperature reaches the melting point.

Due to the difficulty in determining the melting point from experiments, computer simulations are becoming the mainstream method to study the melting behavior of nanoparticles. For example, Monte Carlo (MC) and MD simulations are the most widely used methods to investigate the melting behavior of nanoparticles. However, MC simulation cannot show the true dynamics of a system. Because of the existence of the so-called superheating and undercooling during the computer simulation of melting, the precise determination of the melting point based on conventional MD is also difficult. Accordingly, the lack of accurate melting temperature hinders the development of the thermodynamic model of melting.

In this paper, we adopt REMD,[27] which was proposed to overcome the multiple-minima problem based on replica exchanged method[28,29] and suitable for calculating the thermal properties of clusters,[30] to study the size dependent melting behavior of iron nanoparticles. We find that REMD can determine the melting point much more accurately than by conventional MD. The accurate melting temperatures allow us to make a detail comparison between various melting models.

II. Computational details

We use both REMD and MD methods to study the melting behavior of iron nanoparticles. The many-body potential[31] was used for the Fe–Fe interactions, which is widely used to model crystalline and liquid iron.[32,33] The melting temperature of bulk

[a]*Key Laboratory for Computational Physical Sciences (MOE), State Key Laboratory of Surface Physics, and Department of Physics, Fudan University, Shanghai 200433, China*
[b]*Department of Physics, East China Normal University, Shanghai 200062, China*

iron is about 1772 K based on this model potential, in comparison with 1812 K experimental value. Numerous particles, Fe_N, with N being 272, 523, 958, 1977, 4069, 7983, 15022 and 29585, were simulated by REMD. The initial structures were approximately spherically cut from the bulk phase, and then relaxed at a temperature below the melting point. In the REMD and MD simulations, the time step for integration is one femtosecond (fs), and the NVT ensemble is applied. All the simulations are performed by using the LAMMPS code.[34]

The REMD is successful in overcoming the quasi-ergodicity because it could simultaneously simulate different temperatures (replicas) and exchange each other according to the Metropolis criterion. REMD[27] could be generally described as the following: there are M non-interacting replicas in the generalized ensemble. Initially, each replica is in the canonical ensemble at M different temperatures T_{cm} ($m = 1,\ldots,M$). When a pair of replicas i and j exchange their temperature $T_m = (1/k_B\beta_m)$ and $T_n = (1/k_B\beta_n)$, the generalized ensemble state X will be changed to X'. According to the detailed balance condition, the transition probability $\omega(X \rightarrow X')$:

$$W_{REM}(X)\omega(X \rightarrow X') = W_{REM}(X')\omega(X' \rightarrow X) \quad (1)$$

where $W_{REM}(X)$ and $W_{REM}(X')$, the weight factor in this generalized ensemble, are given by the product of Boltzmann factors for each replica for state X and X', respectively. To fulfil the detailed balance, $\omega(X \rightarrow X')$ can be given by:[27]

$$\omega(X \rightarrow X') = \omega(x_m^{[i]} | x_n^{[j]}) = \begin{cases} 1, & \text{for } \Delta \leq 0 \\ \exp(-\Delta), & \text{for } \Delta > 0 \end{cases} \quad (2)$$

where

$$\Delta \equiv [\beta_n - \beta_m](E(q^{[i]}) - E(q^{[j]})), \quad (3)$$

where $E(q^{[i]})$ and $E(q^{[j]})$ are the potential energy of replica i and j, respectively.

In our simulation, 60 temperatures were used for relatively small nanoparticles (272, 523, 958 and 1977 atoms) and 36 temperatures were used for larger systems (4069, 7983, 15022 and 29585 atoms) in REMD. The temperatures were selected near the melting point. The time step was set to 1 fs, the total simulation time of each replica was 5 ns (5×10^6 timesteps), which were exchanged every 2 ps. For each temperature (replica), the physical quantities (energy, *etc.*) were averaged within the last 2 ns. For each sweep of 2 ps, the first ps is used for the equilibrium of the system, and only the second ps is used for statistics.

To demonstrate the efficiency of REMD, the Fe_{523} was studied in detail by both conventional MD and REMD. In conventional MD, for different temperatures, the simulations were performed with different simulation times (0.5 ns, 5 ns, 10 ns, 100 ns) in the heating and cooling processes. For each simulation, we use only the second half for the statistics, such as averaging of the total energy. With different simulation times, we can clearly see the superheating and undercooling phenomena in conventional MD simulations, which is not present in REMD (see below).

III. Results and discussion

We have studied the heating/cooling behavior of Fe_{523} by using conventional MD simulations. The average total energy per atom as a function of temperature with various simulation times are shown in Fig. 1. The superheating and undercooling phenomenon can be obviously observed, indicated by the differences in the melting and freezing points.[35,36] With increasing simulation time, the freezing point increases, and the melting point and freezing point become closer. The difference between the melting point and freezing point is about 360 K with a simulation time of 0.5 ns, and the difference decreases to 20 K with simulation time of 100 ns. From Fig. 1, we can also see that the variation of the freezing point is larger than the melting point for different simulation times. The reason may lie in that liquid states have a more flat potential-energy surface than that in the solid.

Table 1 lists the melting temperature at different simulation times, where the melting point is defined as the average temperature between melting temperature in heating process and freezing temperature in the cooling process. Obviously, the results are dependent on the simulation time. Even with a simulation time of 100 ns, the difference between melting and freezing points is still as large as 20 K. These results indicate that it is very difficult to obtain an accurate melting point by conventional MD, thus a more efficient simulation method is necessary.

Fig. 2 shows the total energy per atom as a function of temperature obtained by the REMD simulations. The jump in the caloric curve indicates the solid–liquid phase transition. The transition temperature T_{cm} = 1237.4 K for Fe_{523} is clearly different to1221 K from MD simulation even for100 ns. One can clearly see that REMD is more efficient than the conventional MD. The reason lies in that the frequent exchange of replicas could exempt the trapping in the local minimum energy states. During the REMD simulation, all the replicas were heated and cooled repeatedly. The algorithm trends to simulate the replica with a higher energy reference structure at higher temperature and *vice versa*. Finally the dividing point of the temperature between the replica with a liquid structure and the replica with a

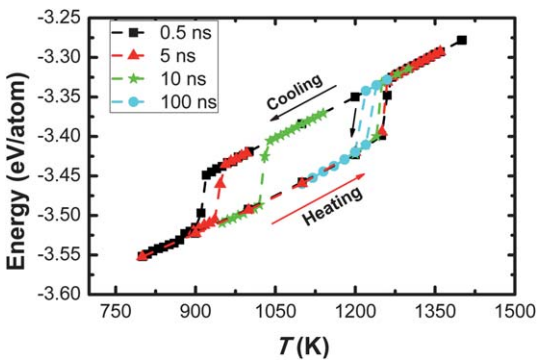

Fig. 1 Average total energy per atom of Fe_{523} as a function of temperature obtained by MD with various simulation times. The black arrows represent the cooling process and the red arrow represents the heating process. The simulation time (per temperature) of 0.5 ns (squares), 5 ns (upwards triangle), 10 ns (star), 100 ns (circles) was simulated in both heating and cooling processes. The difference between the melting point (obtained from the heating process) and freezing point (obtained from the cooling process) decreases with the simulation time increasing.

Table 1 The melting temperature of Fe_{523} in different simulation time at each temperature was acquired by MD. The melting temperature T_m becomes larger when increasing the simulation time

Time (ns)	0.5	5	10	100
T_m (K)	1084	1101	1135	1221

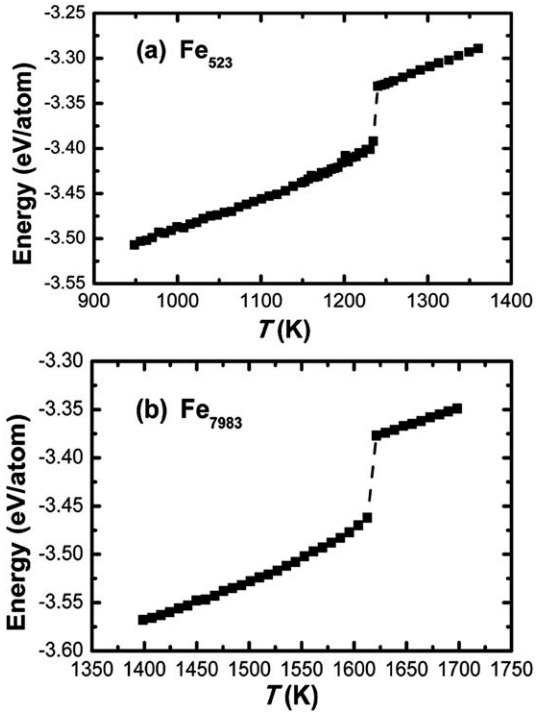

Fig. 2 Average total energy per atom as a function of the temperatures obtained by the REMD for Fe_{523} (a) and Fe_{7983} (b). REMD can effectively avoid the superheating and undercooling phenomena.

solid structure is around the melting point. Therefore, the superheating and undercooling phenomena,[14,35,36] which exist in MD simulations, would effectively be overcome.

Similarly by using REMD, we have determined the melting temperature of a series of iron nanoparticles. The obtained melting points are T_{cm} = 1064.3 K, 1348.2 K, 1474.5 K, 1564.4 K, 1618.6 K, 1656.9 K and 1681.2 K for Fe_{272}, Fe_{958}, Fe_{1977}, Fe_{4069}, Fe_{7983}, Fe_{15022} and Fe_{29585}, respectively (see Fig. 3).

With the accurately determined melting temperature, we are able to revisit various melting models, such as the HGM and LSM model. Fig. 3 shows the reduced melting temperature of Fe nanoparticles as a function of the inverse radius. We have fitted the melting temperature by using both the HGM and LSM models. The fitted results are also shown in Fig. 3.One can see that, the calculated data can be fitted by the LSM model in the whole range of sizes of nanoparticles, while the HGM model fails. This indicates that the melting temperature is not a simple linear function of $1/R$. The better fitting of the LSM model suggests that the surface melting should exist in iron nanoparticles. Carefully comparing the REMD data with the fitting to the LSM model, one can see the fitting is far from the perfect, the deviation at larger nanoparticles clearly exists. The reason could be the fixed thickness of surface liquid layer used in the LSM model, as discussed later.

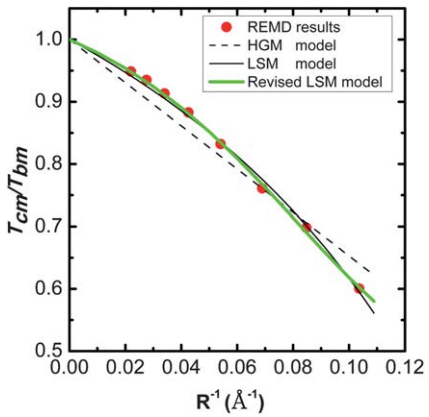

Fig. 3 The reduced melting temperature as a function of the inverse radius. T_{cm} is the melting point of nanoparticles and T_{bm} (1772 K) is the melting point of bulk.[31] The red-circles are the REMD results, and the dash, black and green lines represent the HGM, LSM and revised LSM model. The LSM and revised LSM model can be better fitted to the REMD simulation results, and the revised LSM is little better than LSM model.

To check the melting behavior further, we have studied the surface melting, by calculating the Lindemann index which is very useful quantity for describing the surface melting. Taking Fe_{1977} as an example, we have calculated the Lindemann index of each atom. The Lindemann index[37] of each atom and each shell to characterize solid–liquid transition is expressed as:

$$\delta_i = \frac{1}{N-1}\sum_{j(\neq i)} \frac{\sqrt{\langle r_{ij}^2\rangle_T - \langle r_{ij}\rangle_T^2}}{\langle r_{ij}\rangle_T}, \quad (4)$$

$$\delta_s = \frac{1}{n}\sum_{i\in shell} \delta_i \quad (5)$$

where δ_i is the Lindemann index of each atom, r_{ij} is the distance between the i^{th} and j^{th} atoms and $\langle\ldots\rangle_T$ denotes the average over time at temperature T. To explicitly describe the local melting, the cluster was divided into concentric shells with the same thickness (2 Å). Atoms can be assigned to each shell according to the distance to the mass center. δ_s is the Lindemann index of each shell, where the summation is taken over all the atoms in the corresponding shell. N is the number of atoms in the nanoparticle and n is the number of atoms in the corresponding shell.

According to eqn (4) and (5), we calculated the Lindemann index of each shell at different temperatures. The Lindemann indices for all shells in the Fe_{1977} nanoparticles are shown in Fig. 4. When the temperature is far below the melting point, the Lindemann index is very small for each shell, which suggests that the nanoparticle is in the well-defined solid state. As the temperature increases up to a certain temperature below the melting point, δ_s of the surface shell begins to increase remarkably and is much bigger than the inner shells. This means that the atoms near the surface are more diffusive than the inner atoms, which is an indication of surface melting. When the temperature further increases to 1480 K, δ_s for each shell becomes homogeneous and very large. It indicates that, at the temperature of 1480 K, the nanoparticle is in a well-defined liquid state. We can

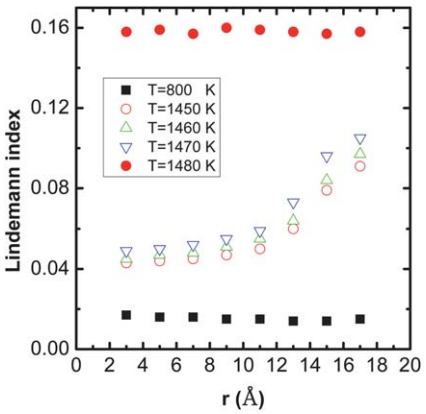

Fig. 4 Radial distribution of the Lindemann index of Fe_{1977} as a function of r (average distance from center of mass of each shell) at different temperatures. The temperatures of 800 K (squares), 1450 K (open circles), 1460 K (open upwards triangle), 1470 K (open downwards triangle) and 1480 K (filled circles) are calculated. The surface melting clear exists from 1450 K, 1460 K and 1470 K. When the temperature up to 1480 K, the Lindemann indices in the whole regions suddenly increase, suggesting the melting at temperature near 1480 K.

conclude that surface melting is occurring in the iron nanoparticles. From Fig. 4, one also can see that the liquid layer does not grow with temperature before full melting. Similar behavior is also observed in all the studied nanoparticles. This is why the LSM model can be employed to describe size dependency of such melting behavior.

The thickness of surface melting layers can be estimated from the change of Lindemann index with respect to the distance from the mass center. We determine the boundary of surface liquid layer in which the Lindemann index begins to increase dramatically. The thickness of liquid layer (σ) is about 7.0 Å for Fe_{1977}. The thickness of liquid layer for various sizes (σ) obtained by the same method is shown in Fig. 5.One can see that, the thickness of liquid layer is not a constant; in contrast to the well accepted

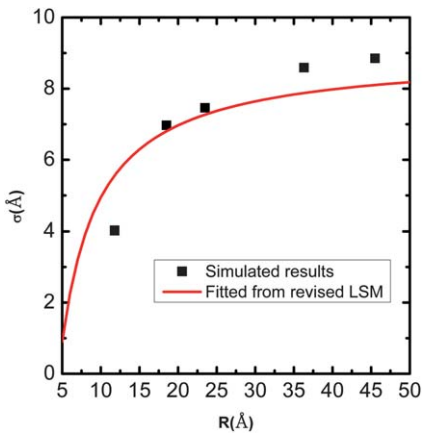

Fig. 5 The thickness of the liquid layer σ as a function of the radius R. Black squares represent the results from the Lindemann index analysis from our simulated data. The red line is the fitted thickness of liquid surface layer according to revised LSM with a size dependent σ, as shown eqn (6). The fitted results from melting temperature to the revised LSM are in agreement with the calculated thickness from the simulated data.

assumption as a constant, it changes with nanoparticle sizes. We propose a relation between σ and the radius of the nanoparticles as follows:

$$\sigma = \frac{a}{R} + b, \tag{6}$$

where a and b are constant. Substituting eqn (6) into LSM, we can obtain $a = -40.45$ Å^2, $b = 8.99$ Å by fitting the REMD melting temperature data, as shown in Fig. 3. Comparing the LSM fitting, the revised LSM with size dependent σ gives a much better fitting in the whole region, which rationalized the revision of the LSM by introducing a size dependent σ, instead of constant σ as used in the literature.[22,38] Furthermore, the fitted σ from revised LSM, as shown in Fig. 5, is also in agreement with what we calculate from the Lindemann index.

IV. Conclusion

With the REMD method, we have studied the size dependent melting behavior of iron nanoparticles. We find that the REMD can accurately determine the melting points, which effectively overcome superheating and undercooling. While the calculation of melting points by conventional MD is time consuming, the superheating and undercooling can hardly be avoided. By calculating the Lindemann index, we find the coexistence of a solid core and a liquid shell, and sudden melting of the solid core takes place when the temperature reaches the melting point. Moreover, the thickness of the surface liquid layer is not a constant but changes with the size of nanoparticles. With accurate determination of melting temperature and the thickness of the liquid layer, we show that the size dependence of nanoparticle melting can be qualitatively described by a revised LSM, in which the change of thickness of surface liquid layer is incorporated.

Acknowledgements

This work is partially supported by the Special Funds for Major State Basic Research, National Science Foundation of China, Ministry of Education and Shanghai Municipality. The calculations were performed in the Supercomputer Center of Shanghai, the Supercomputer Center of Fudan University.

References

1 D. Astruc, F. Lu and J. R. Aranzaes, *Angew. Chem.*, 2005, **117**, 8062.
2 R. Narayanan and M. A. El-Sayed, *J. Am. Chem. Soc.*, 2003, **125**, 8340.
3 G. Bertsch, *Science*, 1997, **277**, 1619.
4 M. Schmidt, R. Kusche, W. Kronmüller, B. von Issendorff and H. Haberland, *Phys. Rev. Lett.*, 1997, **79**, 99.
5 M. Schmidt, R. Kusche, B. von Issendorf and H. Haberland, *Nature*, 1998, **393**, 238.
6 R. Kusche, Th. Hippler, M. Schmidt, B. von Issendorff and H. Haberland, *Eur. Phys. J. D*, 1999, **9**, 1.
7 S. L. Lai, J. Y. Guo, V. Petrova, G. Ramanath and L. H. Allen, *Phys. Rev. Lett.*, 1996, **77**, 99.
8 T. Bachels and H. J. Guntherodt, *Phys. Rev. Lett.*, 2000, **85**, 1250.
9 E. A. Olson, M. Y. Efremov, M. Zhang, Z. Zhang and L. H. Allen, *J. Appl. Phys.*, 2005, **97**, 034304.
10 L. J. Lewis, P. Jensen and J.-L. Barrat, *Phys. Rev. B: Condens. Matter*, 1997, **56**, 2248.
11 A. Barybin and V. Shapovalov, *J. Appl. Phys.*, 2011, **109**, 034303.
12 S. Valkealahti and M. Manninen, *Z. Phys. D: At., Mol. Clusters*, 1993, **26**, 255.

13 D. J. Wales and R. S. Berry, *J. Chem. Phys.*, 1990, **92**, 4283.
14 Y. Shibuta and T. Suzuki, *Chem. Phys. Lett.*, 2007, **445**, 265.
15 H. Duan, F. Ding, A. Rosén, A. R. Harutyunyan, S. Curtarolo and K. Bolton, *Chem. Phys.*, 2007, **333**, 57.
16 J. Kang, S. H. Wei and Y. Kim, *J. Am. Chem. Soc.*, 2010, **132**, 18287.
17 D. Y. Sun and X. G. Gong, *Phys. Rev. B: Condens. Matter*, 1998, **57**, 4730.
18 P. Pawlow, *Z. Phys. Chem.*, 1909, **65**, 1; P. Pawlow, *Z. Phys. Chem.*, 1909, **65**, 545.
19 P. Pawlow, *Z. Phys. Chem.*, 1910, **74**, 562.
20 Ph. Buffat and J.-P. Borel, *Phys. Rev. A: At., Mol., Opt. Phys.*, 1976, **13**, 2287.
21 K. J. Hanszen, *Z. Phys.*, 1960, **157**, 523.
22 C. R. M. Wronski, *Br. J. Appl. Phys.*, 1967, **18**, 1731.
23 P. R. Couchman and W. A. Jesser, *Nature*, 1977, **269**, 481.
24 K. K. Nanda, S. N. Sahu and S. N. Behera, *Phys. Rev. A: At., Mol., Opt. Phys.*, 2002, **66**, 013208.
25 M. Wautelet, *J. Phys. D: Appl. Phys.*, 1991, **24**, 343.
26 K. K. Nanda, *Pramana*, 2009, **72**, 617.
27 Y. Sugita and Y. Okamoto, *Chem. Phys. Lett.*, 1999, **314**, 141.
28 R. H. Swendsen and J.-S. Wang, *Phys. Rev. Lett.*, 1986, **57**, 2607.
29 K. Hukushima and K. Nemoto, *J. Phys. Soc. Jpn.*, 1996, **65**, 1604.
30 Y. Zhai, A. Laio, E. Tosatti and X.-G. Gong, *J. Am. Chem. Soc.*, 2011, **133**, 2535.
31 M. I. Mendelev, S. Han, D. J. Srolovitz, G. J. Ackland, D. Y. Sun and M. Asta, *Philos. Mag.*, 2003, **83**, 3977.
32 D. Y. Sun, M. Asta, J. J. Hoyt, M. I. Mendelev and D. J. Srolovitz, *Phys. Rev. B: Condens. Matter Mater. Phys.*, 2004, **69**, 020102.
33 D. Y. Sun, M. Asta and J. J. Hoyt, *Phys. Rev. B: Condens. Matter Mater. Phys.*, 2004, **69**, 174103.
34 S. J. Plimpton, *J. Comput. Phys.*, 1995, **117**, 1.
35 R. S. Berry, *Sci. Am.*, 1990, **263**, 68.
36 Y. Shibuta and T. Suzuki, *J. Chem. Phys.*, 2008, **129**, 144102.
37 F. A. Lindemann, *Z. Phys.*, 1910, **11**, 609.
38 Y. G. Chushak and L. S. Bartell, *J. Phys. Chem. B*, 2001, **105**, 11605.